Draft version August 15, 2020
Typeset using LaTeX **twocolumn** style in AASTeX63

Periods and Classifications of RR Lyrae stars in M15

Andrew M. Hoffman,[1,2,*] Yukei S. Murakami,[1,2,†] WeiKang Zheng,[1] Benjamin E. Stahl,[1,2,‡] and Alexei V. Filippenko[1,3]

[1] *Department of Astronomy, University of California, Berkeley, CA 94720-3411, USA*
[2] *Department of Physics, University of California, Berkeley, CA 94720-3411, USA*
[3] *Miller Senior Fellow, Miller Institute for Basic Research in Science, University of California, Berkeley, CA 94720, USA*

(Dated: August 15, 2020)

ABSTRACT

We present measurements of the periods, amplitudes, and types for 78 RR Lyrae stars in the globular cluster M15 derived from Nickel telescope observations conducted at Lick Observatory in 2019 and 2020. Of these, two were previously reported but without a determination for the period. In addition, we identify five Cepheid variable stars for which we report three novel period determinations, and a further 35 stars with uncertain classifications and periods. We discuss the development and subsequent application to our data of a new Python package, Period-determination and Identification Pipeline Suite (PIPS), based on a new adaptive free-form fitting technique to detect the periods of variable stars with a clear treatment of uncertainties.

Keywords: globular clusters: individual (M15) – stars: evolution – stars: variables: other

1. INTRODUCTION

Pulsating variable stars periodically change their brightness over timescales ranging from a few hours to a few months, making them members of a select group of astronomical objects that are dynamic over time intervals that are observable by humans (Percy 2007). Moreover, the observable details of this dynamic behavior follows patterns that are unique to each type of variable star, a property that makes photometric time-series analysis a particularly useful tool for their study (Budding & Demircan 2007).

The astrophysical applications of variable star observations span many fields, e.g., testing hydrodynamical models (Smolec & Moskalik 2012) and investigating the expansion of the Universe (Scolnic et al. 2019), and their utility is often limited by the quality of their period determinations. If the measurement of a variable star's period is uncertain, this error can propagate into many other "downstream" facets of an analysis — accuracy is, therefore, critical.

RR Lyrae variable stars are evolved low-mass stars which have moved off the main sequence onto the horizontal branch. They are among the most common types of variable stars in the Universe, especially in galactic globular clusters (Clement et al. 2001). Despite a large number of samples and a long history of observations (from Pickering et al. 1901 to e.g. Pietrukowicz et al. 2020), the behavior of RR Lyrae stars is not fully understood. For instance, the expected long-term behavior is not agreed upon nor immediately evident in observations. Stars do not remain on the horizontal branch forever, but the degree, timescale, and type of evolution within the branch is not trivial to theorize or measure. Observations spanning large temporal ranges (~ 100 yr) suggest that RR Lyrae stars have generally stable periods (Arellano Ferro et al. 2018), but some theories predict noticeable changes (Fadeyev 2018). Moreover, the short-term modulation of light curves (Blažko 1907) seen in some stars remains an open question. Recent studies (Bryant 2015) suggest that the multi-mode property of such "Blazhko stars" resembles known multi-mode RR Lyrae stars (RRd), and studies connecting them are needed.

When studying RR Lyrae stars it is valuable for repeated observations to be made as often as possible. Such observations yield (among other things) a basis with which to investigate long-term changes and may yield insights into the multi-mode behavior of RRd stars, which can then be used to study other multi-mode be-

* andrewmh@berkeley.edu
† sterling.astro@berkeley.edu
‡ Marc J. Staley Graduate Fellow.

haviors, such as Blazhko stars. Messier 15 (NGC 7078, M15) is well suited for such studies. It is an old and star-dense globular cluster (Mészáros et al. 2020) that contains many evolved star types, and in particular, dozens to hundreds of RR Lyrae stars which can be well resolved by telescopes of moderate size. Many photometric observations of RR Lyrae stars in M15 can be found in the literature, including (Bailey et al. 1919; Wemple 1932; Mannino 1956; Makarova & Akimova 1965; Sawyer Hogg 1973; Filippenko & Simon 1981; Bingham et al. 1984; Silbermann & Smith 1995; Corwin et al. 2008; Arellano Ferro et al. 2006; Siegel et al. 2015).

In this paper we present new observations of RR Lyrae stars in M15 and an analysis of their types and pulsation periods. In section 2 we discuss our observation and data processing methods, including our use of the Nickel telescope at Lick observatory on Mt. Hamilton. We also discuss matching the variable stars detected from raw data with known catalog variable stars. Then, in section 3, we discuss our method of detecting the period of observed variable stars, with an emphasis on dealing with widely spaced data, and also discuss our methods of handling error propagation and star classification. In section 4 we present the periods, magnitudes, and type classification of 78 RR Lyrae stars recovered from our observations and derived by our analysis. We also highlight several stars for which few or no previous detections exist, discuss a number of additional stars for which we were not able to accurately determine periods, and briefly discuss period determinations for a small number of Cepheid variable stars. We give conclusions and directions for future work in Section 5.

2. OBSERVATION AND DATA REDUCTION

2.1. *Observations*

Over approximately one year, we obtained 691 images of M15 on 46 nights using the 1-meter Nickel telescope, located at the the Lick observatory on Mt. Hamilton, CA. We observed M15 for an average of 20 minutes per observation night, with a typical time between observations of roughly 7 days. As RR Lyrae stars have typical oscillation periods of between 0.2 and 0.9 days (Corwin et al. 2008), our observing cadence produces widely scattered data when compared to the pulsation period. Ideally, fast pulsators such as RR Lyraes should be observed as often as possible to capture the full range of behavior (VanderPlas 2018). With widely scattered data, period determination becomes difficult, as does avoiding aliasing.

After considering the field of view of the Nickel telescope, we chose to take 4 tiled fields of M15 in order to image the largest number of stars. The arrangement is shown in Fig. 1. Our typical field observations consist of exposures of 20, 60, and 180 seconds in the V-band. This strategy increases the likelihood of obtaining at least one data point per night with a sufficiently high signal-to-noise ratio (SNR), given the varying brightness of our targets. When time permits, images are also taken in the B-band.

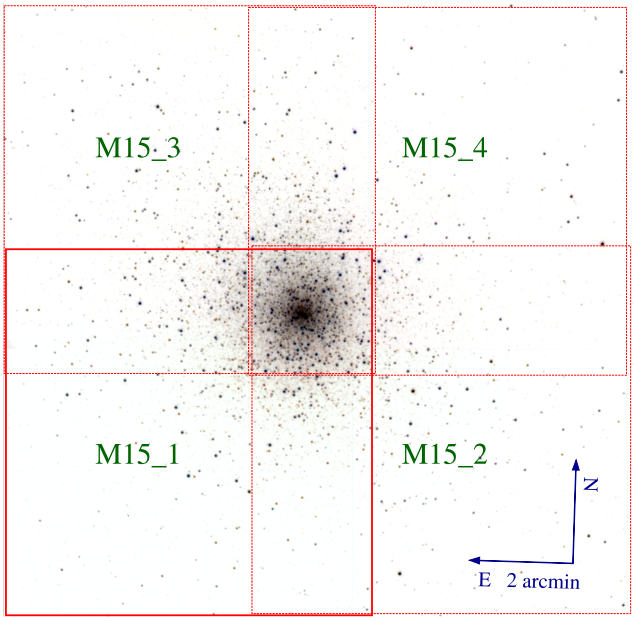

Figure 1: Tiled images of M15, with each being a BVR composite of inverted-color Nickel telescope images. Our observations cover 10×10 arcmin centered at the core of M15 by combining four tiled images (M15_1 – M15_4) that each have a $\sim 6 \times 6$ arcmin field.

With a plate scale of 0.368 arcsec/pixel[1], the core of M15 is sometimes not well resolved in our images. Because of this, there are limitations in period determinations for stars which are located close to the core. When looking through previously published data, we see a similar trend where stars which are harder to individually resolve are less likely to have reported periods (e.g., Siegel et al. 2015). To minimize the effect of this issue, tiled fields are overlapped at the core, increasing the chance of detection by collecting a larger number of data points.

2.2. *Data Reduction*

2.2.1. *LOSSPhotPypeline*

To convert images from the Nickel telescope into Landolt-system photometry and subsequently, light

[1] We use 2×2 binning with the 2048×2048 CCD whose normal plate scale is 0.184 arcsec/pixel.

Field	$N_{\rm stars}$	$\overline{\Delta V}$ (mag)	$(\Delta V)_{\rm max}$ (mag)	$\overline{\sigma V}$ (mag)	$(\sigma V)_{\rm max}$ (mag)
M15_1	9	−0.0002	0.0242	0.0170	0.0319
M15_2	9	−0.0004	0.0157	0.0162	0.0303
M15_3	8	−0.0004	0.0346	0.0218	0.0340
M15_4	10	−0.0012	0.0210	0.0192	0.0245

Table 1: Statistics for calibration stars used in each field. $N_{\rm stars}$ is the number of calibration stars in each field. ΔV is the deviation from the corresponding PS1 magnitude and σV is the observed standard deviation, both in the V-band.

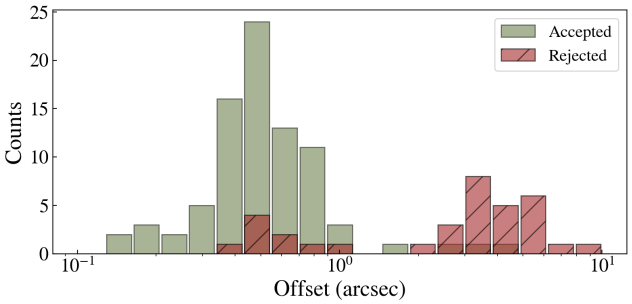

Figure 2: Offset of our candidate stars from GCVS catalog θ_i, in arcsec.

curves, we utilize the LOSSPhotPypeline[2] (LPP; Stahl et al. 2019). The LPP provides robust methods for uncertainty calculation, including reduction on simulated stars in the field. We use these uncertainties as a proxy by which to identify poor quality data that need to be removed from further analysis. As our use of the LPP is consistent with Stahl et al. (2019), we defer to their Section 3 for a more detailed discussion of its capabilities.

2.2.2. *Calibration*

We calibrate each field by picking bright, non-variable stars that have minimal (typically < 0.03 mag) deviation from the corresponding PS1 catalog values and small (also typically < 0.03 mag) scatter (per calibration star) in each of their observed magnitudes through the entire time series. The first criterion ensures calibration consistency between the four different fields in our tiling strategy (see Fig. 1), and the second — in conjunction with the requirement that only those calibration stars that are detected in every image for a given field be used — ensures a consistent calibration for images taken across large time intervals. After calibration, we set a 0.03 mag floor on magnitude uncertainties (commensurate with our second criterion). We summarize important statistics for our calibration choices in Table 1, while detailed information is relegated to Table 3 in the Appendix.

2.2.3. *Cross-matching*

We identify candidate variable stars using the LPP's ability to automatically detect all resolvable stars in an image. For each field, this procedure identifies ~ 1300 candidates, which we then compare to previously published positions for variable stars. Specifically, we calculate the angular distance between star i identified by the LPP and star j in Samus' et al. (2017) (GCVS), $\theta_{ij} = \cos^{-1}\left[\sin(\delta_i)\sin(\delta_j)+\cos(\delta_i)\cos(\delta_j)\cos(\alpha_i-\alpha_j)\right]$. Here, α is the right ascension and δ is the declination of the subscripted object, both in radians. Once this 2d-array is generated, we take $\min(\theta_j)_i$ to create a list of the variable stars nearest to each candidate. This list contains many duplicates, so we further narrow it by taking $\min(\min(\theta_j)_i)_j$ for each duplicate star j. The resulting list contains each star's coordinates (α and δ), ID, and the offset from the relevant GCVS star. This process is repeated for all four fields, M15_1 to M15_4. Our star ID is expressed with 'V' numbers (e.g., V001). This is a modified version of older notations, such as V1, as seen in Bailey (1902) and other papers. After this process, we obtain ~ 60 candidate stars in each field to be processed.

Since there are overlaps between each field, we process stars in more than one field whenever possible, thereby allowing us to choose the data based on various quality parameters (see Sec. 3.1). The resulting, cross-matched catalog shows strong agreement with GCVS coordinates. There are two populations, one with a small (~ 0.4 arcsec) offset and one with a larger (~ 2.5 arcsec) offset, which can be seen in Fig. 2. Our final selections (see Sec. 4) suggest that stars in the second (large-distance) population mostly fail to provide high quality data. Assuming GCVS has high accuracy, this is the expected result.

3. ANALYSIS

3.1. *PIPS*

We have developed the Period-determination and Identification Pipeline Suite (PIPS)[3], a new Python package to analyze variable star data. While there are many algorithms and code bases available for this purpose, we found that several improvements were needed

[2] https://github.com/benstahl92/LOSSPhotPypeline

[3] https://github.com/SterlingYM/PIPS

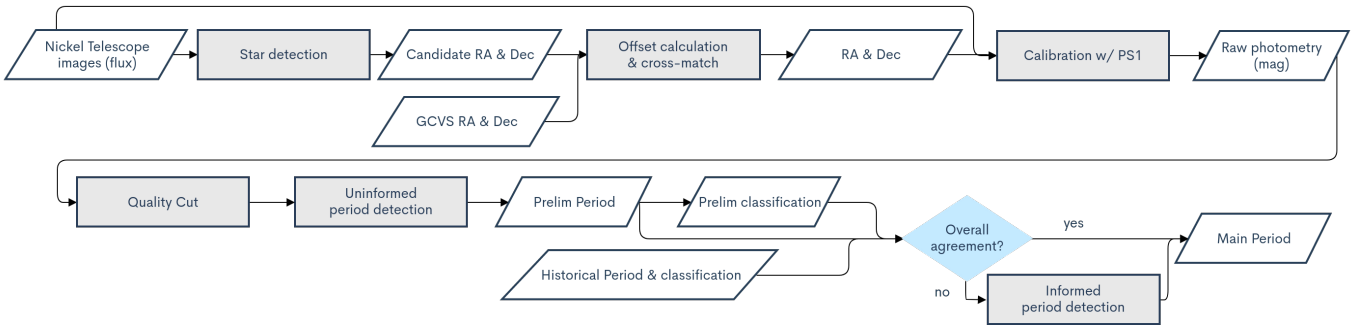

Figure 3: Data reduction process chart.

to obtain the best results, especially for difficult objects characterized by widely spaced data, low SNR, and few data points.

3.1.1. *Motivation and Background*

Period Uncertainty—We note that in older publications, particularly in studies which rely on the time of maximum light (see, e.g., Bailey 1902; Wemple 1932; Makarova & Akimova 1965), uncertainty quantification is not treated carefully. More recently, the method of fitting to folded data instead of relying on the maximum or minimum times has become more prominent (see Holl et al. 2018), and with it, a clearer understanding and treatment of uncertainty. This is of great importance for modern studies as long-term data can and will be used to study the evolution of certain quantities (e.g., period and metallicity), and a careful treatment of uncertainty is required for proper error propagation and the statements of confidence that such calculations support. In developing PIPS, our primary concern was therefore to examine the uncertainty created when making period determinations.

Template Bias—When analyzing variable star photometry, our goal is to determine the period and create analytic functions (e.g., Fourier series) which provide an accurate description of the star's light curve. Although high cadence observations can yield a complete light curve and through it, a direct measurement of the period, data is often[4] taken with a lower cadence. This necessitates phase folding to obtain a light curve (VanderPlas 2018), and therefore requires a determination of the period before analysis can proceed. The principle challenge in our work is then to break the degeneracy between the period and the light curve.

The Lomb-Scargle periodogram is the most common algorithm designed to detect sinusoidal signals in widely or unevenly spaced data (VanderPlas 2018). Template Fourier Fitting (TFF Kovács & Kupi 2007) is a technique which leverages high cadence data of similar phenomena to create an informed prior for light curve fitting. Both of these techniques can make period determinations, but the bias induced by one's choice of light curve template is not widely addressed.

Due to Lomb-Scargle's nature as a correlation function to a sinusoidal pattern (Lomb 1976; Scargle 1982), taking the maximum returned power value only yields the best fit period to a sinusoidal wave. Because light curve shapes are not sinusoidal past first or second order[5], this sinusoidal dependence is analogous to the template dependency in TFF. Both the template dependency in TFF and the sinusoidal dependence in LS skew results from these methods. The RRab subtype of RR Lyrae stars, for instance, have sharply peaked maxima which are poorly described by a sinusoid (e.g., light curves in Corwin et al. 2008). For this reason, we employ a template-free fitting method with PIPS to minimize bias.

3.1.2. *Methodology*

PIPS is a period determination algorithm based on template-free, adaptive function ('Free-Form') fitting. The analysis begins with an initial guess from the Lomb-Scargle periodogram, but proceeds to refine the value and explore the associated error. We assume that when a light curve is folded about a more correct period, fitting will yield a smaller χ^2 value compared to a folding about a value farther from the true pulsation period. We also assume that there will be one global minimum when examining the χ^2 space, representing the true period of the star. The simplest way to find this correct period would be to iterate through the entirety of possible periods and perform a fit to the data folded with each period in turn. This is computationally intensive, inefficient, and complicates the exploration of uncertainty. We choose instead to provide an informed prior based on

[4] For instance, many modern all-sky surveys.

[5] Or in some cases, even less — see RRab type stars.

the Lomb-Scargle estimation, and use χ^2 minimization where both the period and the Fourier terms are free parameters. We find that this identifies the period more accurately and that this exploration of parameter space provides robust information regarding the uncertainty of the value.

Given time series data, PIPS finds the best value for the principle pulsation period by checking χ^2 values against the best-fit Fourier function which represents the analytic form of light curve,

$$y_{\rm fit} = A_0 + \sum_{k=i}^{K_{\rm max}} \left[a_k \sin\left(\frac{2\pi k}{P} x\right) + b_k \sin\left(\frac{2\pi k}{P} x\right) \right]. \tag{1}$$

Here, x is the phase-folded time data $x \equiv t \pmod P$, and $y_{\rm fit}$ represents the expected magnitude at that phase (unitless phase is x/P). The parameters A_0, a_k, b_k, and P, are determined by a linear regression fitting using the `curve_fit` function in `scipy` (Virtanen et al. 2020). In this analysis, we take $K_{\rm max} = 5$, based on a cross-validation test using Gaia data of RR Lyrae stars.

The number of parameters and intrinsic scatter (or a small SNR) may in some cases make it difficult to fit the correct value of P. This is primarily because Fourier parameters dominate the degrees of freedom, yielding many local minima in the χ^2-space when viewed as a function of P. Additionally, the change in the χ^2 value at different P becomes less obvious as the SNR gets smaller, because even at the best-P, the folded data exhibit a roughly correct shape but with large intrinsic scatter, yielding a relatively large χ^2 value. These relations can be viewed as analogous to the mechanics of a potential well whose surface is the representation of the χ^2 value. This well exhibits a larger friction force between sliding objects as the surface becomes rougher (many local minima) due to different combinations of Fourier coefficients. The SciPy `curve_fit` function attempts to 'place an object' (the initial guess) to perform tests with the goal of finding the 'bottom' of the well. How far this test object slides down is a function of the slope. This 'slide test' tends to be unsuccessful near the bottom of the potential, which can be seen in a near one-to-one relationship between the initial guess and the resulting 'best fit' period. The 'initial kick' from the linear regression algorithm yields a characteristic size in the scatter of the resulting period when compared to the initial guess values, and we take this as the statistical uncertainty of the period

$$\sigma_P = \mathrm{std}\left(P_{\rm fit} - P_{\rm trial}\right)\Big|_{P_{\rm trial}\sim P}. \tag{2}$$

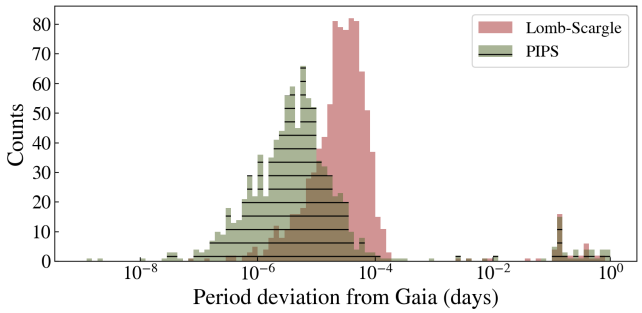

Figure 4: Deviation from Gaia period (ΔP) when analyzed with Lomb-Scargle (red) and PIPS (green).

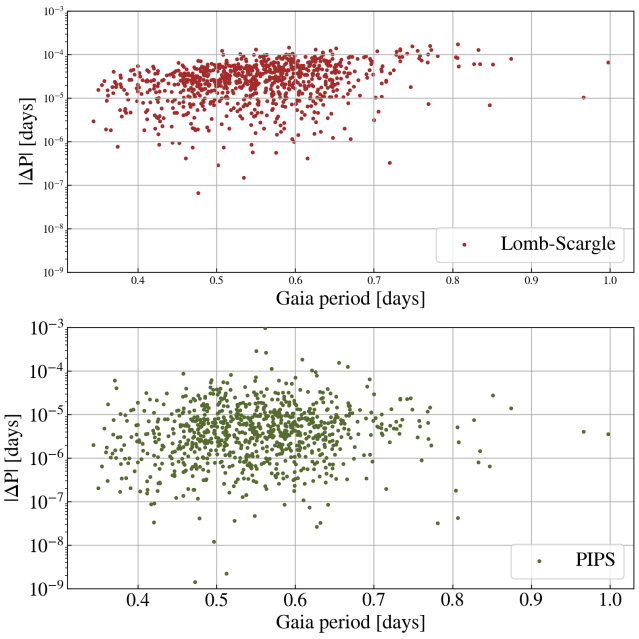

Figure 5: $|\Delta P|$ as a function of Gaia's period, for our stars with $\Delta P < 10^{-2}$ only. Lomb-Scargle shows a slight correlation between period and error, while our pipeline is more consistent across a large range of periods.

This process requires a fitting to Eq. 1 between $10^2 - 10^4$ times, and our pipeline is designed to perform this analysis as fast as possible. When the uncertainty of the period is not required, it is sufficient and much faster to find the P which yields a minimum χ^2 for Eq. 1 when evaluated as a function of P (i.e., fixed P within single fitting).

3.1.3. *Performance validation*

We tested the period-detection function of our pipeline with raw RR Lyrae light curves from Gaia DR2 (Holl et al. 2018). We chose a sample consisting of 1355 RR Lyrae stars (`gaiadr2.vari_rrlyrae`). This set of data includes 910 RRab stars and 445 RRc or RRd stars,

whose photometry in G-band is taken for more than 30 epochs (`num_clean_epochs_g`>30) and is located nearby (`parallax`>0.25) with less than 20% error in its astrometry measurement (`parallax_over_error`>5). We search for any period between 0.2 and 1.0 days equally without an initial guess, with no visual inspection or human help.

The results for this validation are shown in Figures 4 and 5. In most cases both Lomb-Scargle (LS) and PIPS agreed with Gaia's period, although there is a population with $\sim 0.1 - 1.0$ days error in period values. About 96% of LS results and 95% of PIPS results were considered 'good results', and PIPS outperforms LS with mean error an order of magnitude smaller than LS results. Moreover, LS exhibits a slight correlation between ΔP and period, an expected behavior when a non-informed uniform prior in frequency space is used. This creates non-equally-spaced windows in period space and thus the resolution becomes lower as the period gets larger. PIPS adaptively changes the search window size, and therefore does not exhibit this issue.

Since Lomb-Scargle is a widely accepted tool in the community, we consider our new package PIPS as an equally acceptable tool overall and one which may be better suited for our particular analysis based on these validation results.

3.2. *Classification*

RR Lyrae stars are generally classified based on their pulsation modes. This classification was first introduced by Bailey (1902), and other than the consolidation of RRa and RRb type stars into the RRab type, it has remained the accepted method. RR Lyrae subtypes are largely separated by the fundamental mode pulsation with RRab (also called RR0) having a 0.5−0.7 day period and the first overtone pulsation, RRc (RR1), having a $\sim$ 0.3 day period. Some stars exhibit a combination of these two modes, and are classified as RRd (RR01). The fundamental mode generally has a steep rise in magnitude, while the first overtone is closer to a sinusoid. The shapes of these light curves are explained using a mechanical/mathematical model in Stellingwerf et al. (1987). RRab stars sometimes exhibit a significant modulation in amplitude at a period of a few weeks to a year. This phenomenon is called the "Blazhko effect" after the first observation (see Blažko 1907), and several attempts have been made to explain it (Bryant 2015). The existence of other higher modes and combinations of such modes (i.e., the existence of 'RRe' stars) is still an area of active discussion.

In order to classify the stars in our sample, we follow the general methodology seen in most RR Lyrae star and M15-specific studies (e.g., Clementini et al. 2016; Silbermann & Smith 1995). Although the original method to distinguish between RRab and RRc stars is morphology-based and requires a careful statistical study of population and various parameters, it is now clear that RRab stars can be distinguished from RRc and RRd stars clearly in period space. This is especially true in M15, whose member objects share similar metallicities and ages (Mészáros et al. 2020). This prior knowledge about a narrow range of metallicities resolves the possible degeneracy that arises between different Oosterhoff groups (Oosterhoff 1939).

Our procedure to classify variable stars follows three steps: (1) based on existing studies, we confirm that the distribution of our detected periods agrees with those in the literature, (2) determine the separation between types, and (3) confirm the overall agreement in various parameter spaces. Figure 7 shows the distribution of detected periods and amplitudes. As reported in Oosterhoff (1939) and Silbermann & Smith (1995), we see a gap between the two main populations at a period value of roughly 0.5 days.

Once the initial classification based on the main period is finished, we search for the secondary period to distinguish between RRc and RRd stars. This analysis is based on two assumptions: (a) RR Lyrae stars pulsate in either the fundamental mode (with period P_f) or the first overtone (with period P_1), where $P_1/P_f \sim 0.75$ (see Holl et al. 2018), and (b) the period is either P_f or P_1 and can be distinguished based on the primary period value. First, the photometry data V is naively separated into two functions:

$$V = A_0 + A_1 \sin\left(\frac{2\pi}{P_1}t - \phi_1\right) + A_f \mathcal{F}\left(\frac{2\pi}{P_f}t - \phi_f\right), \quad (3)$$

where $\mathcal{F}$ is a template Fourier function that generates an RRab-type curve. This template is taken from our own RRab stars that show minimal scatter and have near-even coverage across phase space. Subscript X_0 refers to the zeroth-order constant value. Similarly, X_1 is for the first overtone, and X_f is the fundamental mode in each term. We focus on finding the secondary pulsation near the expected ratio $P_1/P_f \sim 0.74$ following the definition of RRd stars used in Clementini et al. (2016), but we do not apply any cuts based on this ratio. This model is chosen based on our knowledge that RRd stars exhibit a combination of RRab and RRc star properties (e.g.,

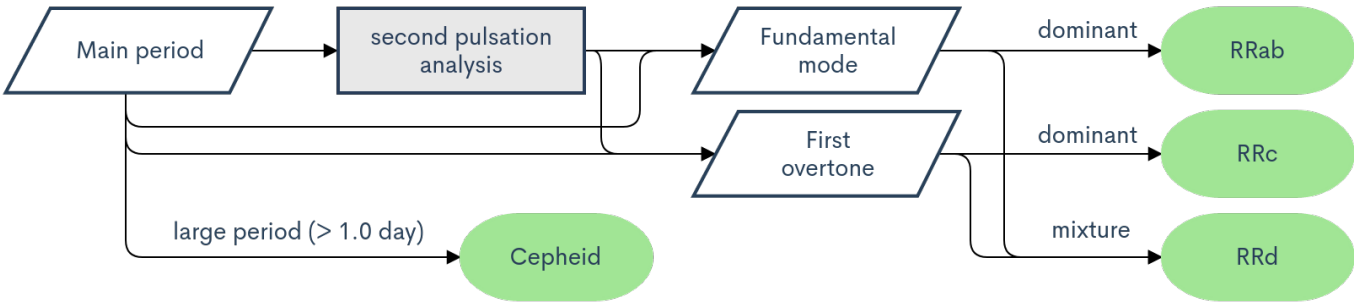

Figure 6: A flowchart showing the procedure to classify variable stars.

Jurcsik & Hajdu 2017), and that RRc stars are near-sinusoidal[6].

Once this preliminary fitting has yielded rough estimates of the parameters A_i, ϕ_i, and P_i, we then take the 'unknown' component from the original data. For example, $V_1 = V - A_0 - A_f\mathcal{F}\,(2\pi t/P_f - \phi_f)$ is calculated for RRab candidates to search for a first-overtone component. This component is then processed with our period detection function to find a period value. Although the model Eq .3 cannot remove all of the fundamental mode components from the data, it is important that majority of the component pulsating in P_f is removed, so that the less obvious pulsation in P_1 can be detected. When the period is determined, we fit a function

$$V = A_0 + A_1\mathcal{F}_1\left(\frac{2\pi}{P_1} - \phi_1\right) + A_f\mathcal{F}_f\left(\frac{2\pi}{P_f} - \phi_f\right) \quad (4)$$

with the newly obtained best-fit Fourier functions $\mathcal{F}_1$ and $\mathcal{F}_f$. These Fourier functions are specific to each object, and are created by several iterations of fitting, subtracting from raw data, and fitting again; this alternation between two modes followed by re-creation of the other mode mostly removes the bias introduced by Eq. 3. While this method is fast and effective for a small amount data, or stars with poor SNR, these secondary components are only to be used as a classification reference. Any in-depth analysis of secondary pulsation at a different ratio (e.g., Bryant 2015) requires more complete data and/or a full treatment of the complex shape.

While the majority of RRab stars show a large value of A_f/A_1, our results suggest that many of our RRc candidates have a large secondary pulsation in the fundamental mode. These pulsations show amplitudes comparable to the main pulsation in the first overtone, and are classified as RRd stars. The resulting population distribution is discussed in Sec. 4.

4. RESULTS

[6] It should be noted that this method does not eliminate or distinguish between binary systems with one RRab star, which would exhibit a combination of sinusoidal and RRab-like curves.

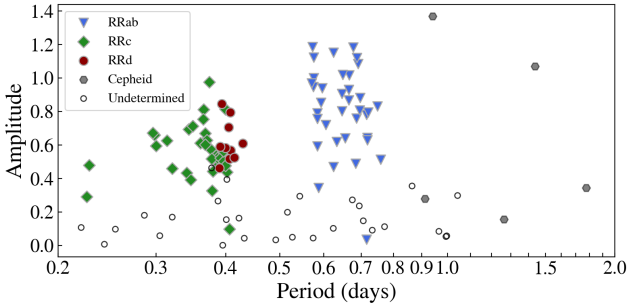

Figure 7: Classification based on the Bailey (period-amplitude) diagram. These data are used to make initial guesses for the dominant component in the double mode analysis. RRd stars whose type is determined after double mode analysis are overlayed.

4.1. *Period Determinations*

We have determined periods and types for 83 variable stars, of which 78 were RR Lyrae stars and five were Cepheid stars. The results of our analysis are presented in Table 2, which includes the ID, position, best-fit period determination and its uncertainty, amplitude, and type classification for each star we considered. The period error is determined by taking the largest uncertainties out of three sources: instrumental (telescope timestamp), statistical (randomness in the fitting algorithm), and algorithmic (insufficient χ^2 search scaling) errors. We believe that the resulting errors ($\sim 10^{-7}$ days) are more accurate and meaningful than many previously reported uncertainties, which are generally calculated by taking the instrumental timestamp uncertainty divided by the number of periods spanned during observations. Unless otherwise noted, we do not accept data above an error threshold $\sigma_V \geq \sigma_{V,\mathrm{cut}}$, where $\sigma_{V,\mathrm{cut}} = \overline{\sigma_V} + \mathrm{std}(\sigma_V)/2$. We show our phase-folded light curves in Figures 10–14, with the addition of two decomposed pulsation modes for double-mode RRd stars.

4.2. *Stars by Type Classification*

Out of 78 total variable stars, we find 36 RRab type stars, with an average period of 0.65 days. These stars

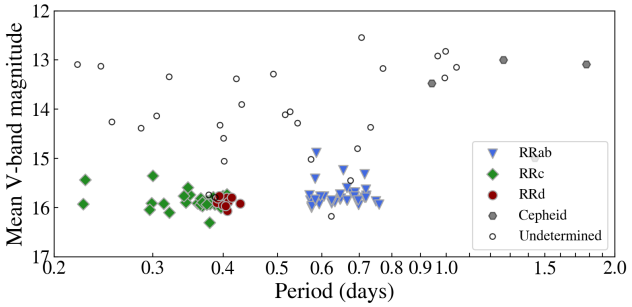

Figure 8: Mean V-band magnitude of star and main pulsation period of each star. Cepheid stars are well isolated from RR Lyrae stars, and the higher magnitude of undetermined stars suggests contamination from nearby stars.

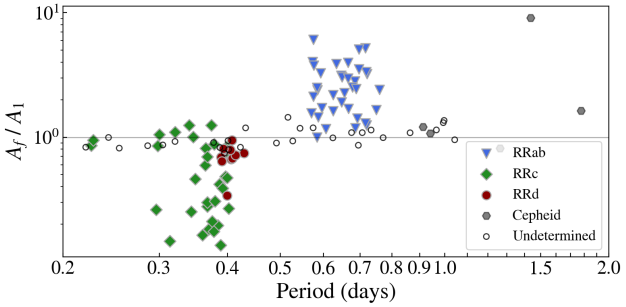

Figure 9: Main pulsation period and Af/A1, the ratio between the amplitudes of the fundamental mode and the first overtone.

are clearly distinguished by their sharply peaked maxima and are single-mode pulsators[7]. We classify 33 stars as RRc with an average period of 0.35 days, and with light curves showing near-sinusoidal shapes unique to first overtone pulsation. We find 10 RRd multi-mode stars with an average period of 0.40 days, although we note that this period value is specific to the first overtone when considering multi-mode pulsators. While less common in M15, we also detect 5 Cepheid variables, with an average period of 1.26 days. These Cepheid light curves are similar to RRab stars, as they pulsate in the fundamental mode, but their forms vary and we do not perform a detailed analysis of them. We made 34 possible detections of variable stars, in addition to the 78 about which we are confident. This undetermined population typically belongs to the 'large distance' group identified in Fig. 2 and are not firmly classified due to possible contamination and a small SNR. We mark uncertain stars as '??'.

The overall population distribution in the Bailey (period-amplitude) diagram (Fig.7) shows some notable characteristics, such as *(a)* a short pulsation ($\sim 0.2-0.4$ days) with a relatively small amplitude ($\lessapprox$ 0.9 mag) for RRc stars, *(b)* a narrow period range for RRd stars ($P \sim 0.39-0.41$ days), *(c)* no confirmed detections of variable stars near $P \sim 0.5$ days, and *(d)* RRab stars having a wide range in amplitude ($0.4-1.3$ mag) but a small range in period ($P \sim 0.55-0.75$ days). These characteristics are consistent with the statistics found in large surveys, such as Holl et al. (2018).

When our stars are plotted in period-magnitude space as seen in Fig. 8, all types of RR Lyrae stars are tightly gathered at a similar apparent V-band magnitude of $V \approx 16$ mag. This is consistent with previous observations (e.g., Bingham et al. 1984; Silbermann & Smith 1995), and clearly shows the separation of Cepheid stars from RR Lyrae stars, which are brighter and have longer pulsation times. Our undetermined stars are often brighter, and there is no consistency in their measured periods, which span values belonging to all RR Lyrae types as well as Cepheids. This suggests that the majority of the undetermined stars are contaminated by nearby objects, raising their perceived brightness but leaving a wide range of period values.

Examining the ratio of the two decomposed pulsation mode amplitudes can show a clear separation between RR Lyrae star types, which were mainly classified by period. In Fig. 9, the relationship of the period and the ratio between the amplitudes of the fundamental mode and first overtone is shown. Stars with an A_f/A_1 value greater than one are dominated by the fundamental mode, which is clearly seen in the population distribution of RRab stars. RRc stars, which are dominated by the first overtone, are clearly seen as having an A_f/A_1 value less than one. The multi-mode pulsator RRd stars, however, are overall much closer to the value $A_f/A_1 = 1$, showing that both pulsation modes are present. We note that most RRd stars have in general an A_f/A_1 value slightly less than one, suggesting that the first overtone is slightly more dominant in most RRd stars.

The ratio of the periods of the fundamental mode and the first overtone is also a notable feature of the multi-mode RRd stars. Prior works suggest that this ratio should be quite narrow (see Clementini et al. 2016), and our results support this with bounds of $0.7451 \leq P_1/P_f \leq 0.7502$ and a mean value for P_1/P_f of 0.7463.

[7] Note that these distinguishing features are not used for classification, but that the clear differences support classification via separation in period-amplitude space.

4.3. *Notes on individual stars*

V027—We can confirm that V27 does not appear be a variable star, as has been noticed since at least Sawyer Hogg (1973).

V095—This variable has a period of 1.263 days, and peaks brighter than 13th magnitude. No period determinations for this star can be found in the reference literature, likely due to brightness contamination resulting from close proximity to the core of M15. The period and brightness of this star suggest that is it a Cepheid variable.

V107—Both the light-curve shape and the period of 0.277 days suggest that it is an RRc type RR Lyrae star. No previous determinations for the period can be found in the reference literature.

V123—While the light-curve shape is unclear, the period of 0.715 days and the magnitude range suggest that this is an RRab type RR Lyrae star. No previous determinations for the period can be found in the reference literature.

V140—This variable also peaks brighter than 13th magnitude and has a relatively long period of 1.776 days, suggesting that it too is a Cepheid variable. No previous determinations for the period can be found in the reference literature.

V155—Another bright star with a long period of 0.912 days, this variable is also likely a Cepheid, and also does not have a previous period determination in the reference literature.

Possible detections—Of those variables without classifications, we have detected 10 objects with no previously reported periods in our references. Stars V079, V106a, V106b, V110, V115, V121, V143, V147, V150, V154, and V158 belong to this category. V106a shows a large secondary period, suggesting it is a possible RRd star. These stars require further confirmation and investigation.

5. CONCLUSION AND FUTURE WORK

Using the Nickel Telescope at Lick Observatory, we observed M15 over 46 nights and accumulated 691 images. In tandem, we have developed a custom pipeline to detect periodic behavior in our data. We compared this new, purpose-built pipeline to existing techniques using the Gaia data release and found our results to be highly encouraging. We discussed the analysis of single and multi-mode pulsators, as well as the error treatment in our pipeline. Our analysis lead to confident period classifications for 78 RR Lyrae stars in M15, two of which do not have a value listed in the reference literature. Of these 78 stars, the majority (69) were single mode pulsators, which are classified as RRab and RRc type stars.

Looking to the future, we note that the long-term period evolution of RR Lyrae stars is not well constrained by either theory or observation (Jurcsik & Hajdu 2017). The difficulty of making a sufficiently accurate period determination, combined with the long time-scales required to see this change, restrict the effectiveness of observationally constraining this behavior, and theoretical derivations remain challenging (Stellingwerf et al. 1987). Long-term, high-quality data is necessary for investigating the time evolution of RR Lyrae stars. With the addition of the results presented herein, we plan to conduct such an investigation in a subsequent paper (Murakami et al., in prep.)

ACKNOWLEDGMENTS

We acknowledge Josh Bloom and Dan Weisz for thought provoking discussion on period analysis and validation, and Arjun Savel for providing knowledge on data analysis tools. This research made use of Astropy,[8] a community-developed core Python package for Astronomy (Astropy Collaboration et al. 2013; Price-Whelan et al. 2018). We acknowledge generous support from the TABASGO Foundation, Marc J. Staley, Christopher R. Redlich, and the Miller Institute for Basic Research in Science (U.C. Berkeley). Research at Lick Observatory is partially supported by a generous gift from Google. We also thank all student observers involved with the group, and the assistants at Lick Observatory.

REFERENCES

Arellano Ferro, A., García Lugo, G., & Rosenzweig, P. 2006, RMxAA, 42, 75

Arellano Ferro, A., Rosenzweig, P., Luna, A., et al. 2018, Astronomische Nachrichten, 339, 158–167, doi: 10.1002/asna.201813409

Astropy Collaboration, Robitaille, T. P., Tollerud, E. J., et al. 2013, A&A, 558, A33, doi: 10.1051/0004-6361/201322068

Bailey, S. I. 1902, Annals of Harvard College Observatory, 38, 1

Bailey, S. I., Leland, E. F., Woods, I. E., & Pickering, E. C. 1919, Annals of Harvard College Observatory, 78, 195

Bingham, E. A., Cacciari, C., Dickens, R. J., & Pecci, F. F. 1984, MNRAS, 209, 765, doi: 10.1093/mnras/209.4.765

Blažko, S. 1907, Astronomische Nachrichten, 175, 325, doi: 10.1002/asna.19071752002

Bryant, P. H. 2015, ApJ, 802, 52, doi: 10.1088/0004-637X/802/1/52

Budding, E., & Demircan, O. 2007, Introduction to Astronomical Photometry, Vol. 6

Clement, C. M., Muzzin, A., Dufton, Q., et al. 2001, AJ, 122, 2587, doi: 10.1086/323719

Clementini, G., Ripepi, V., Leccia, S., et al. 2016, Astronomy Astrophysics, 595, A133, doi: 10.1051/0004-6361/201629583

Corwin, T. M., Borissova, J., Stetson, P. B., et al. 2008, The Astronomical Journal, 135, 1459, doi: 10.1088/0004-6256/135/4/1459

Fadeyev, Y. A. 2018, Astronomy Letters, 44, 616, doi: 10.1134/S1063773718100018

Filippenko, A. V., & Simon, R. S. 1981, AJ, 86, 671, doi: 10.1086/112934

Holl, B., Audard, M., Nienartowicz, K., et al. 2018, A&A, 618, A30, doi: 10.1051/0004-6361/201832892

Jurcsik, J., & Hajdu, G. 2017, MNRAS, 470, 617, doi: 10.1093/mnras/stx1302

Kovács, G., & Kupi, G. 2007, A&A, 462, 1007, doi: 10.1051/0004-6361:20066050

Lomb, N. R. 1976, Ap&SS, 39, 447, doi: 10.1007/BF00648343

Makarova, V. A., & Akimova, V. P. 1965, Peremennye Zvezdy, 15, 350

Mannino, G. 1956, Mem. Soc. Astron. Italiana, 27, 169

Mészáros, S., Masseron, T., García-Hernández, D. A., et al. 2020, MNRAS, 492, 1641, doi: 10.1093/mnras/stz3496

Oosterhoff, P. T. 1939, The Observatory, 62, 104

Percy, J. R. 2007, Understanding Variable Stars

Pickering, E. C., Colson, H. R., Fleming, W. P., & Wells, L. D. 1901, ApJ, 13, 226, doi: 10.1086/140808

Pietrukowicz, P., Udalski, A., Soszynski, I., et al. 2020, arXiv e-prints, arXiv:2007.05849. https://arxiv.org/abs/2007.05849

Price-Whelan, A. M., Sipőcz, B. M., Günther, H. M., et al. 2018, AJ, 156, 123, doi: 10.3847/1538-3881/aabc4f

Samus', N. N., Kazarovets, E. V., Durlevich, O. V., Kireeva, N. N., & Pastukhova, E. N. 2017, Astronomy Reports, 61, 80, doi: 10.1134/S1063772917010085

Sawyer Hogg, H. 1973, Publications of the David Dunlap Observatory, 3, 6

Scargle, J. D. 1982, ApJ, 263, 835, doi: 10.1086/160554

Scolnic, D., Perlmutter, S., Aldering, G., et al. 2019, Astro2020: Decadal Survey on Astronomy and Astrophysics, 2020, 270. https://arxiv.org/abs/1903.05128

Siegel, M. H., Porterfield, B. L., Balzer, B. G., & Hagen, L. M. Z. 2015, AJ, 150, 129, doi: 10.1088/0004-6256/150/4/129

Silbermann, N. A., & Smith, H. A. 1995, AJ, 110, 704, doi: 10.1086/117555

Smolec, R., & Moskalik, P. 2012, MNRAS, 426, 108, doi: 10.1111/j.1365-2966.2012.21678.x

Stahl, B. E., Zheng, W., de Jaeger, T., et al. 2019, Monthly Notices of the Royal Astronomical Society, 490, 3882–3907, doi: 10.1093/mnras/stz2742

Stellingwerf, R. F., Gautschy, A., & Dickens, R. J. 1987, ApJL, 313, L75, doi: 10.1086/184834

VanderPlas, J. T. 2018, The Astrophysical Journal Supplement Series, 236, 16, doi: 10.3847/1538-4365/aab766

Virtanen, P., Gommers, R., Oliphant, T. E., et al. 2020, Nature Methods, 17, 261, doi: https://doi.org/10.1038/s41592-019-0686-2

Wemple, L. 1932, Harvard College Observatory Bulletin, 889, 9

APPENDIX

A. TABLE

Table 2. Results.

ID	α (deg)	δ (deg)	Period (P) (days)	σP (days)	Amplitude (mag)	$\overline{V}$ (mag)	Type
V001	322.4590	12.1740	1.43783743	3.7e-07	1.07	14.99	Cepheid
V002	322.4438	12.1687	0.684304375	1.6e-07	0.49	15.74	RRab
V003	322.4222	12.1539	0.388720632	8.5e-06	0.48	15.83	RRc
V004	322.4610	12.1216	0.313589117	2.4e-08	0.63	15.92	RRc
V005	322.4646	12.1081	0.384211954	7.2e-08	0.54	15.78	RRc
V006	322.4995	12.1886	0.666015094	1.7e-07	1.02	15.86	RRab
V007	322.4955	12.1879	0.367563437	1.2e-06	0.63	15.97	RRc
V008	322.4924	12.2027	0.646238777	3.9e-06	0.91	15.84	RRab
V009	322.4967	12.2059	0.715282097	5.7e-07	0.78	15.80	RRab
V010	322.5284	12.1680	0.386389721	2.1e-06	0.52	15.93	RRc
V011	322.5416	12.1617	0.34326551	5.5e-08	0.69	15.89	RRc
V012	322.5387	12.1535	0.592875644	5.2e-07	0.85	15.93	RRab
V013	322.5288	12.1485	0.574910937	1.4e-07	0.95	15.98	RRab
V015	322.5164	12.0831	0.584394482	1.6e-07	0.79	15.86	RRab
V016	322.5210	12.2035	0.399195555	3.3e-07	0.81	15.84	RRc
V017	322.5163	12.1981	0.428912296	1.5e-07	0.61	15.92	RRd
V018	322.5145	12.1954	0.367725969	1.0e-07	0.67	15.87	RRc
V019	322.5240	12.2121	0.572306432	1.9e-06	1.19	15.85	RRab
V020	322.5156	12.1648	0.69695872	4.3e-07	0.88	15.95	RRab
V021	322.5023	12.1513	0.648795261	3.6e-06	1.02	15.82	RRab
V022	322.3988	12.1539	0.720230076	1.6e-06	0.80	15.76	RRab
V023	322.5466	12.2388	0.632698496	1.6e-07	0.62	15.89	RRab
V024	322.4624	12.1654	0.369691742	1.1e-07	0.63	15.87	RRc
V025	322.5786	12.1650	0.665318041	6.2e-06	0.93	15.85	RRab
V026	322.4986	12.2595	0.402317102	4.4e-08	0.44	15.94	RRc
V029	322.5385	12.2263	0.575015865	1.5e-05	1.12	16.00	RRab
V030	322.4458	12.1661	0.405998183	8.0e-08	0.52	15.80	RRd
V031	322.4602	12.2352	0.408183108	6.0e-08	0.57	15.88	RRd
V032	322.4781	12.1972	0.60530342	1.3e-07	0.72	15.77	RRab
V033	322.4812	12.1593	0.583940164	3.5e-08	0.76	15.41	RRab
V034	322.4771	12.1521	0.4010	-	0.15	-	??
V035	322.4834	12.1219	0.624546598	2.6e-07	0.47	15.91	RRab
V036	322.4850	12.1447	0.624130821	2.2e-06	1.15	15.85	RRab
V038	322.4950	12.1268	0.375280597	4.2e-08	0.57	15.87	RRc
V039	322.4986	12.1328	0.389551691	5.2e-08	0.46	15.90	RRd
V040	322.5301	12.1351	0.377331483	4.1e-08	0.52	15.92	RRc
V041	322.5107	12.1521	0.391761515	2.5e-06	0.52	15.88	RRc
V042	322.5575	12.1575	0.360188851	5.2e-08	0.61	15.91	RRc
V044	322.5185	12.1685	0.595669649	4.8e-06	0.94	15.77	RRab
V045	322.5116	12.1588	0.67740415	1.9e-06	1.18	15.69	RRab

Continued on next page

Table 2 – continued from previous page

ID	α (deg)	δ (deg)	Period (P) (days)	σP (days)	Amplitude (mag)	$\overline{V}$ (mag)	Type
V046	322.5090	12.1764	0.69144381	3.6e-06	1.08	15.84	RRab
V047	322.5052	12.1664	0.687547509	1.4e-06	1.12	15.69	RRab
V048	322.5093	12.2092	0.364972072	7.2e-08	0.81	15.81	RRc
V049	322.5038	12.2136	0.655186807	4.3e-06	0.64	15.24	RRab
V050	322.5391	12.1954	0.298060627	4.6e-08	0.66	15.91	RRc
V051	322.4942	12.1928	0.396962319	1.3e-07	0.50	15.93	RRc
V052	322.5473	12.1616	0.575654124	3.6e-06	1.00	15.97	RRab
V053	322.4667	12.1365	0.414109598	9.3e-08	0.52	15.79	RRd
V054	322.4956	12.1919	0.399572367	6.1e-08	0.58	15.95	RRd
V055	322.5114	12.1622	0.748671788	3.9e-07	0.83	15.87	RRab
V056	322.5089	12.1676	0.570260593	1.7e-07	0.97	15.75	RRab
V057	322.5141	12.1522	0.349277148	5.6e-08	0.71	15.74	RRc
V058	322.4770	12.1697	0.407285449	9.1e-08	0.79	16.06	RRd
V059	322.5040	12.1769	0.4319	-	0.04	-	??
V060	322.5080	12.1510	0.718689553	3.6e-07	0.64	15.63	RRab
V061	322.4737	12.1558	0.399688532	9.9e-08	0.48	15.77	RRc
V062	322.4724	12.1780	0.3773	-	0.46	-	??
V063	322.5064	12.1760	0.646891427	1.4e-07	0.80	15.73	RRab
V064	322.4795	12.1728	0.364249404	1.2e-07	0.75	15.94	RRc
V065	322.4637	12.1566	0.71819949	4.5e-06	0.63	15.80	RRab
V066	322.4735	12.1362	0.379343054	3.7e-08	0.44	15.93	RRc
V067	322.4682	12.1644	0.404610074	1.2e-07	0.71	15.97	RRd
V068	322.4830	12.1703	0.3874	-	0.26	-	??
V069	322.4822	12.1607	0.586772955	3.0e-07	0.35	14.89	RRab
V070	322.4831	12.1620	0.367582599	7.4e-08	0.60	15.90	RRc
V071	322.4827	12.1631	0.1058	-	0.14	-	??
V072	322.4923	12.1769	0.686283385	2.8e-07	0.76	15.77	RRab
V073	322.4907	12.1724	0.4020	-	0.39	-	??
V074	322.5035	12.1436	0.296010243	4.6e-08	0.67	16.04	RRc
V075	322.4927	12.1578	0.5269	-	0.05	-	??
V076	322.4926	12.1610	0.3207	-	0.17	-	??
V077	322.4898	12.1621	0.7064	-	0.15	-	??
V078	322.4906	12.1806	0.664751545	1.9e-07	0.87	15.60	RRab
V079	322.4986	12.1611	0.2858	-	0.18	-	??
V081	322.4877	12.1650	0.2535	-	0.10	-	??
V082	322.4879	12.1678	0.4919	-	0.03	-	??
V083	322.4982	12.1661	0.5163	-	0.20	-	??
V084	322.4996	12.1634	0.5433	-	0.29	-	??
V086	322.4964	12.1686	0.941440619	5.5e-07	1.37	13.48	Cepheid
V087	322.5010	12.1613	0.7714	-	0.11	-	??
V089	322.4851	12.1666	0.3046	-	0.06	-	??
V090	322.5025	12.1682	0.1520	-	0.68	-	??
V091	322.5110	12.1753	0.3909291	1.2e-07	0.59	15.81	RRd
V092	322.4957	12.1603	0.373886851	8.7e-08	0.97	15.93	RRc
V093	322.5003	12.1587	0.340598884	6.8e-08	0.43	15.76	RRc
V094	322.4946	12.1750	0.3951	-	0.00	-	??

Continued on next page

Table 2 – continued from previous page

ID	α (deg)	δ (deg)	Period (P) (days)	σP (days)	Amplitude (mag)	$\overline{V}$ (mag)	Type
V095	322.4939	12.1559	1.26357749	8.5e-07	0.16	13.00	Cepheid
V096	322.5393	12.2273	0.396360363	9.5e-08	0.56	16.00	RRc
V097	322.4701	12.1753	0.696354571	9.1e-07	0.81	15.85	RRab
V098	322.4735	12.1800	0.6241	-	0.10	-	??
V099	322.5013	12.2209	0.225141886	4.6e-08	0.29	15.93	RRc
V100	322.4969	12.1566	0.320595991	8.0e-08	0.46	16.10	RRc
V102	322.5129	12.1755	0.759381107	1.9e-06	0.51	15.94	RRab
V103	322.4217	12.0908	0.583845056	1.4e-06	0.59	15.84	RRab
V106a	322.4846	12.1701	0.3935	-	0.85	-	??
V106b	322.4840	12.1716	0.9976	-	0.06	-	??
V107	322.4842	12.1604	0.227240473	3.5e-08	0.48	15.43	RRc
V110	322.5022	12.1562	0.6752	-	0.27	-	??
V111	322.5048	12.1674	0.378130163	7.5e-08	0.33	16.30	RRc
V113	322.4947	12.0980	0.406180567	8.3e-08	0.10	15.73	RRc
V114	322.4935	12.1777	0.345933528	9.3e-08	0.39	15.59	RRc
V115	322.4962	12.1647	2.7123	-	0.21	-	??
V116	322.4970	12.1532	0.9657	-	0.08	-	??
V117	322.4992	12.1571	0.9942	-	0.05	-	??
V118	322.4981	12.1821	0.299995772	7.8e-08	0.59	15.35	RRc
V119	322.4975	12.1697	0.7332	-	0.09	-	??
V121	322.4840	12.2093	0.2422	-	0.01	-	??
V122	322.5660	12.1741	0.5741	-	0.04	-	??
V123	322.4289	12.1648	0.715498035	4.3e-06	0.04	15.32	RRab
V129	322.4922	12.1629	0.2201	-	0.11	-	??
V140	322.4943	12.1673	1.77647668	1.1e-06	0.35	13.09	Cepheid
V143	322.4946	12.1612	0.6949	-	0.24	-	??
V145	322.4973	12.1674	0.4226	-	0.16	-	??
V147	322.4958	12.1657	3.0725	-	0.11	-	??
V150	322.4950	12.1715	1.0432	-	0.30	-	??
V154	322.4916	12.1708	0.8643	-	0.40	-	??
V155	322.4907	12.1697	0.911891427	2.7e-07	0.43	14.77	Cepheid
V158	322.4676	12.1031	0.1181	-	0.68	-	??

Table 3: Calibration stars used with LPP. The magnitude values are all in V-band. 'diff' is deviation of observed value ('obs') from PS1 data ('cal').

#	Field	$\alpha_{\rm obs}$ (deg)	$\delta_{\rm obs}$ (deg)	$\alpha_{\rm diff}$ (deg)	$\delta_{\rm diff}$ (deg)	$V_{\rm cal}$ (mag)	$V_{\rm obs}$ (mag)	$V_{\rm diff}$ (mag)	$\sigma V_{\rm obs}$ (mag)
0	M15_1	322.519265	12.127833	0.000105	0.000066	15.273728	15.287983	0.014255	0.014855
1	M15_1	322.561284	12.140017	0.000107	0.000079	15.464006	15.442372	-0.021634	0.012730
2	M15_1	322.523107	12.118028	0.000107	0.000066	15.506678	15.530928	0.024250	0.012090
3	M15_1	322.533446	12.085643	0.000082	0.000070	15.992274	15.963761	-0.028513	0.013641
4	M15_1	322.543151	12.125756	0.000090	0.000072	15.990031	15.979094	-0.010937	0.014745
5	M15_1	322.534900	12.136032	0.000092	0.000070	16.048878	16.052094	0.003216	0.013421
6	M15_1	322.530015	12.109165	0.000103	0.000065	16.478746	16.496761	0.018014	0.019075
7	M15_1	322.554640	12.141452	0.000097	0.000077	16.790747	16.790150	-0.000597	0.020650
8	M15_1	322.567823	12.134789	0.000100	0.000079	17.252762	17.252872	0.000110	0.031925
9	M15_2	322.459429	12.150704	0.000109	0.000056	14.273025	14.260324	-0.012701	0.013764
10	M15_2	322.458902	12.159175	0.000105	0.000055	14.919133	14.922602	0.003468	0.010524
11	M15_2	322.445463	12.140651	0.000109	0.000055	14.930785	14.917324	-0.013461	0.009058
12	M15_2	322.456988	12.156429	0.000100	0.000061	15.089972	15.072546	-0.017426	0.015132
13	M15_2	322.458802	12.131101	0.000093	0.000046	15.189565	15.185824	-0.003741	0.016033
14	M15_2	322.447355	12.151231	0.000096	0.000063	15.412107	15.412935	0.000828	0.010156
15	M15_2	322.451633	12.155373	0.000094	0.000066	15.419053	15.430990	0.011937	0.022853
16	M15_2	322.462334	12.144905	0.000083	0.000051	15.454053	15.469824	0.015771	0.030308
17	M15_2	322.455935	12.140771	0.000115	0.000051	15.496215	15.507713	0.011498	0.018345
18	M15_3	322.521463	12.222239	0.000095	0.000064	14.395865	14.393613	-0.002252	0.014736
19	M15_3	322.519897	12.196303	0.000098	0.000067	14.553714	14.588363	0.034649	0.014014
20	M15_3	322.543955	12.236424	0.000120	0.000077	15.516245	15.496363	-0.019882	0.026960
21	M15_3	322.548378	12.234880	0.000116	0.000082	15.678872	15.663113	-0.015759	0.034030
22	M15_3	322.521121	12.227391	0.000099	0.000068	15.904249	15.909863	0.005614	0.014118
23	M15_3	322.533092	12.203466	0.000118	0.000068	15.965824	15.989238	0.023414	0.027297
24	M15_3	322.536526	12.208844	0.000107	0.000068	15.991126	15.992488	0.001362	0.021195
25	M15_3	322.540593	12.240000	0.000117	0.000073	16.044006	16.013488	-0.030518	0.022373
26	M15_4	322.448676	12.204609	0.000102	0.000045	14.526760	14.510128	-0.016632	0.015407
27	M15_4	322.448944	12.191813	0.000106	0.000057	15.115295	15.136328	0.021032	0.014781
28	M15_4	322.445159	12.195775	0.000119	0.000055	15.254565	15.249278	-0.005288	0.014280
29	M15_4	322.457367	12.208246	0.000083	0.000051	15.447569	15.461878	0.014309	0.013821
30	M15_4	322.435704	12.192173	0.000132	0.000054	15.380196	15.364628	-0.015568	0.023735
31	M15_4	322.464925	12.212959	0.000096	0.000056	15.770203	15.753778	-0.016425	0.020545
32	M15_4	322.469867	12.195119	0.000086	0.000062	15.896890	15.904128	0.007238	0.024449
33	M15_4	322.437433	12.198128	0.000116	0.000048	16.264444	16.270178	0.005733	0.024551
34	M15_4	322.456705	12.210754	0.000098	0.000048	15.987055	15.979578	-0.007477	0.018576
35	M15_4	322.457820	12.194107	0.000090	0.000065	16.547810	16.548878	0.001068	0.022561

B. LIGHTCURVES

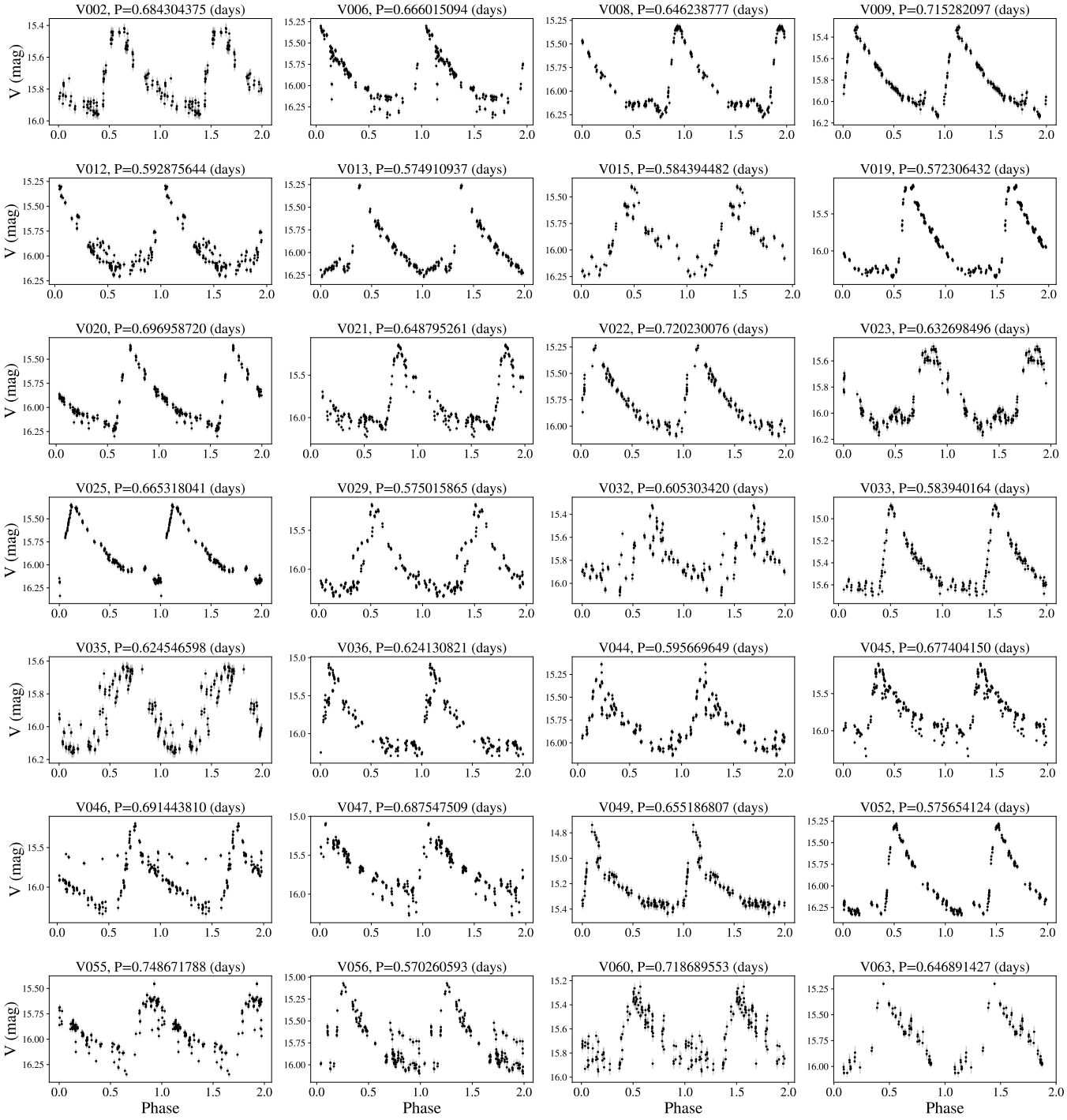

Figure 10: RRab stars: each cell is a folded light curve of a single-mode star pulsating in the fundamental mode (RRab). X-axis is phase (normalized to single period and repeated twice), and Y-axis is observed V-band magnitude.

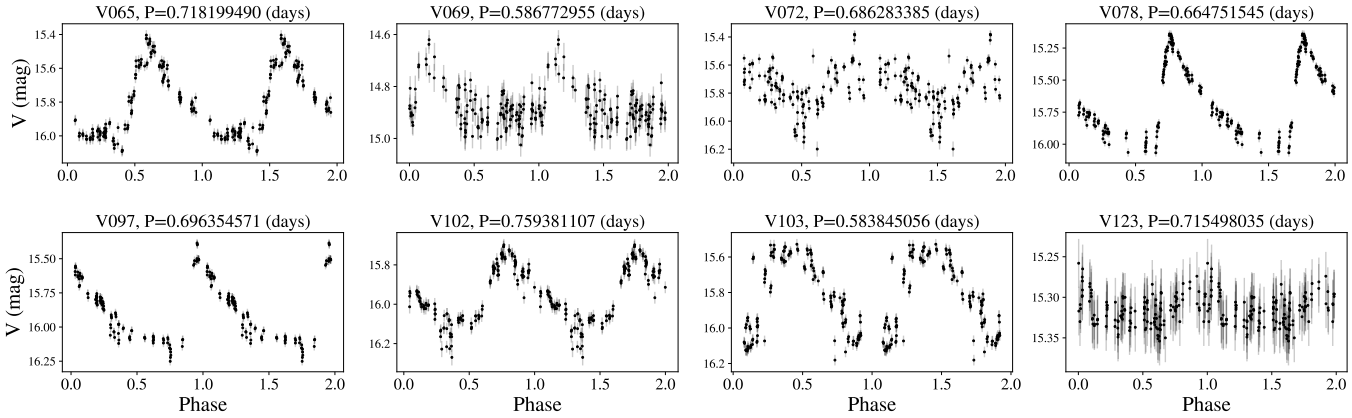

Figure 10: RRab stars (continued)

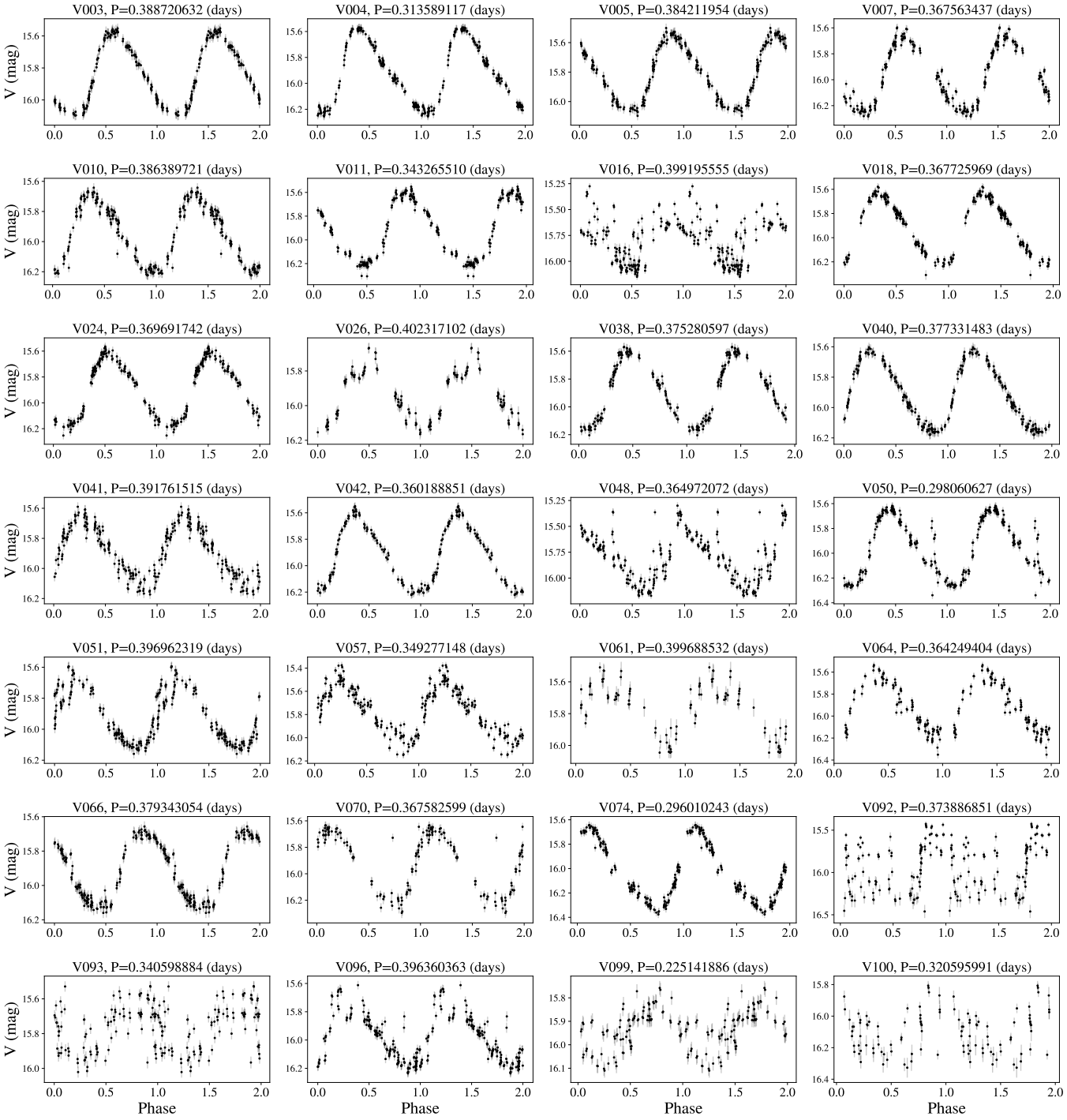

Figure 11: RRc stars. Conventions are the same as in Figure 10.

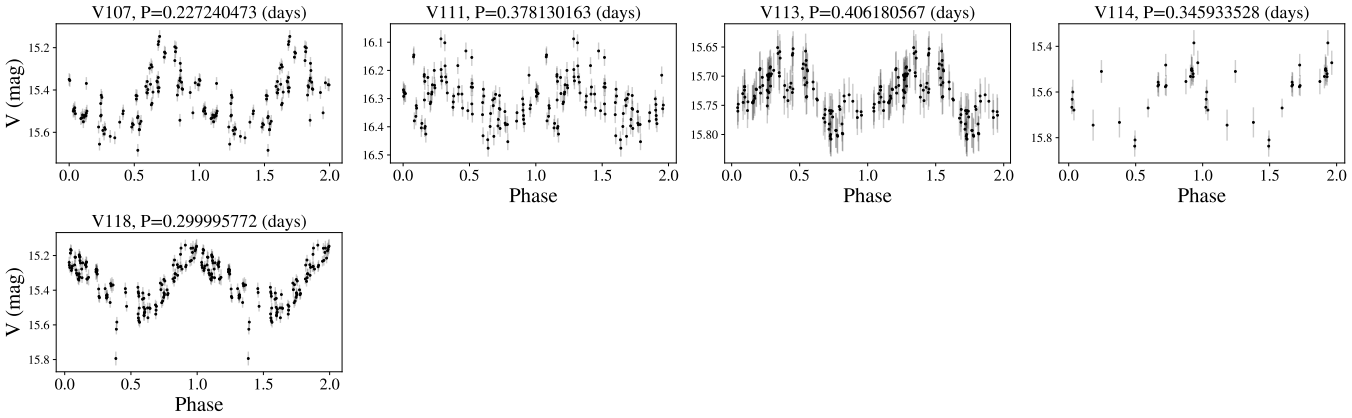

Figure 11: RRc stars (continued)

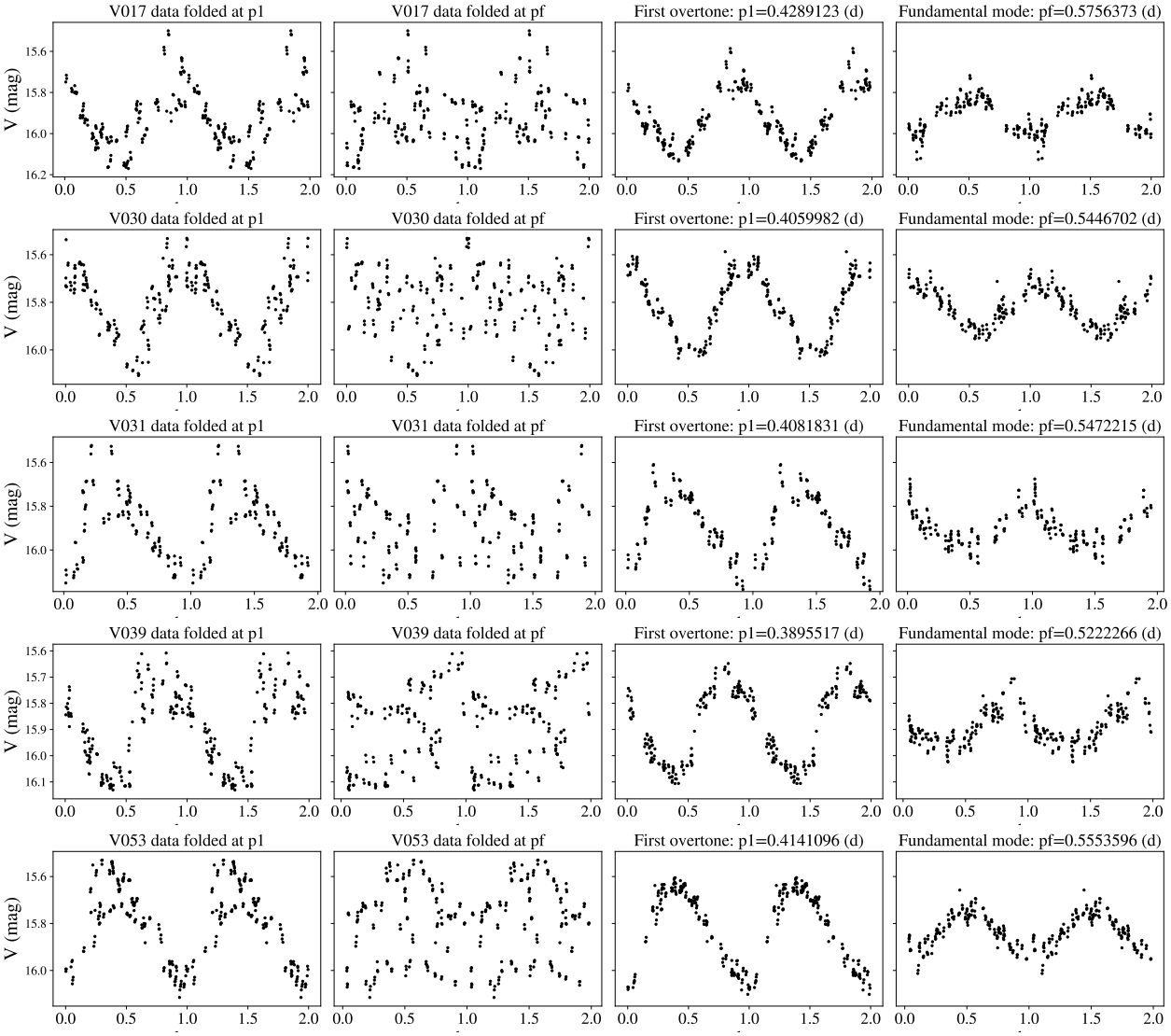

Figure 12: RRd stars: each row represents a star pulsating in two periods simultaneously (RRd). The left two columns show raw data folded at the first overtone period (p1) and the fundamental mode period (pf), and the right two columns represent decomposed multi-mode components. The amplitude of these decomposed pulsations indicates which mode is dominant.

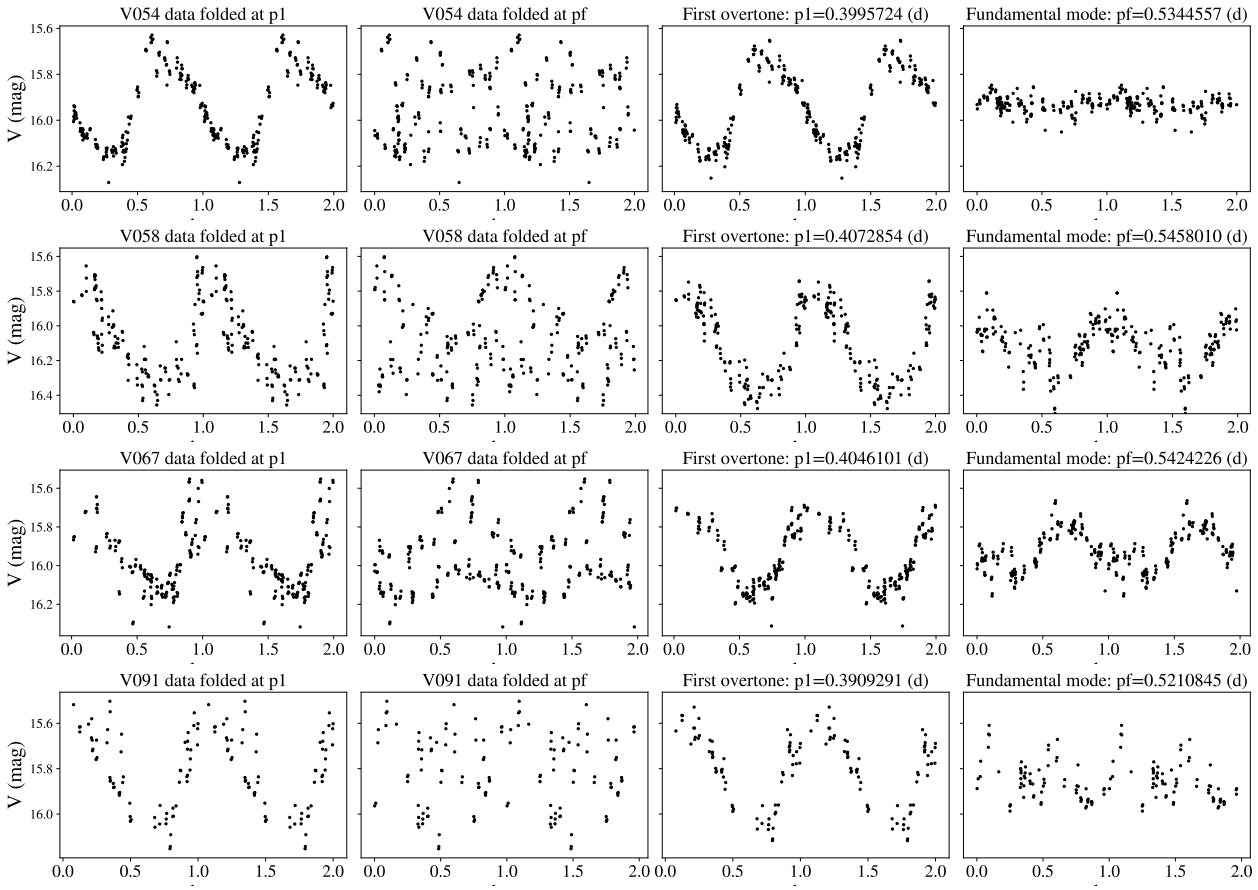

Figure 12: RRd stars (continued)

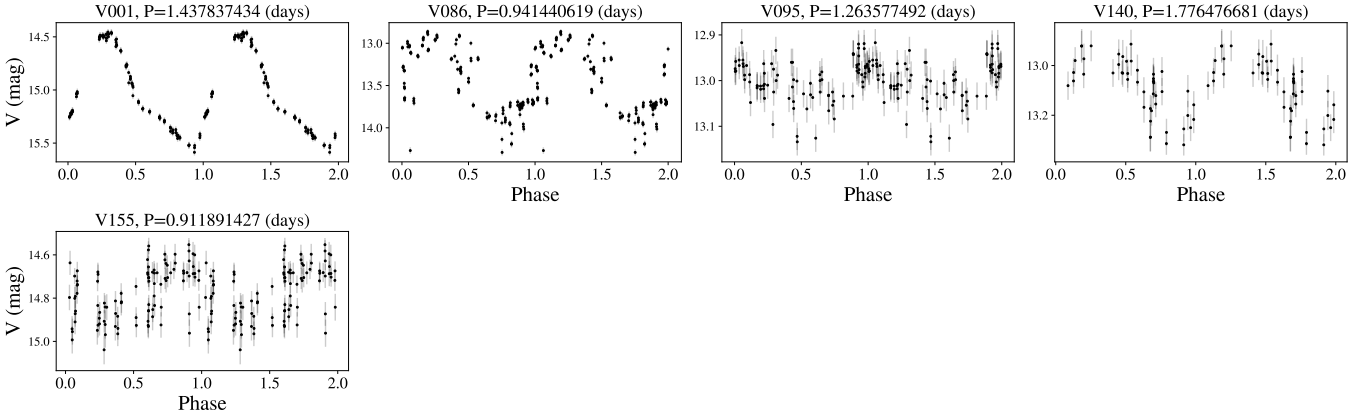

Figure 13: Cepheid stars: each cell is a folded light curve of a single-mode star pulsating in fundamental mode. While these stars exhibit similar morphological characteristics as RRab stars, these stars are brighter and have larger period values. X-axis is phase (normalized to single period and repeated twice), and Y-axis is observed V-band magnitude.

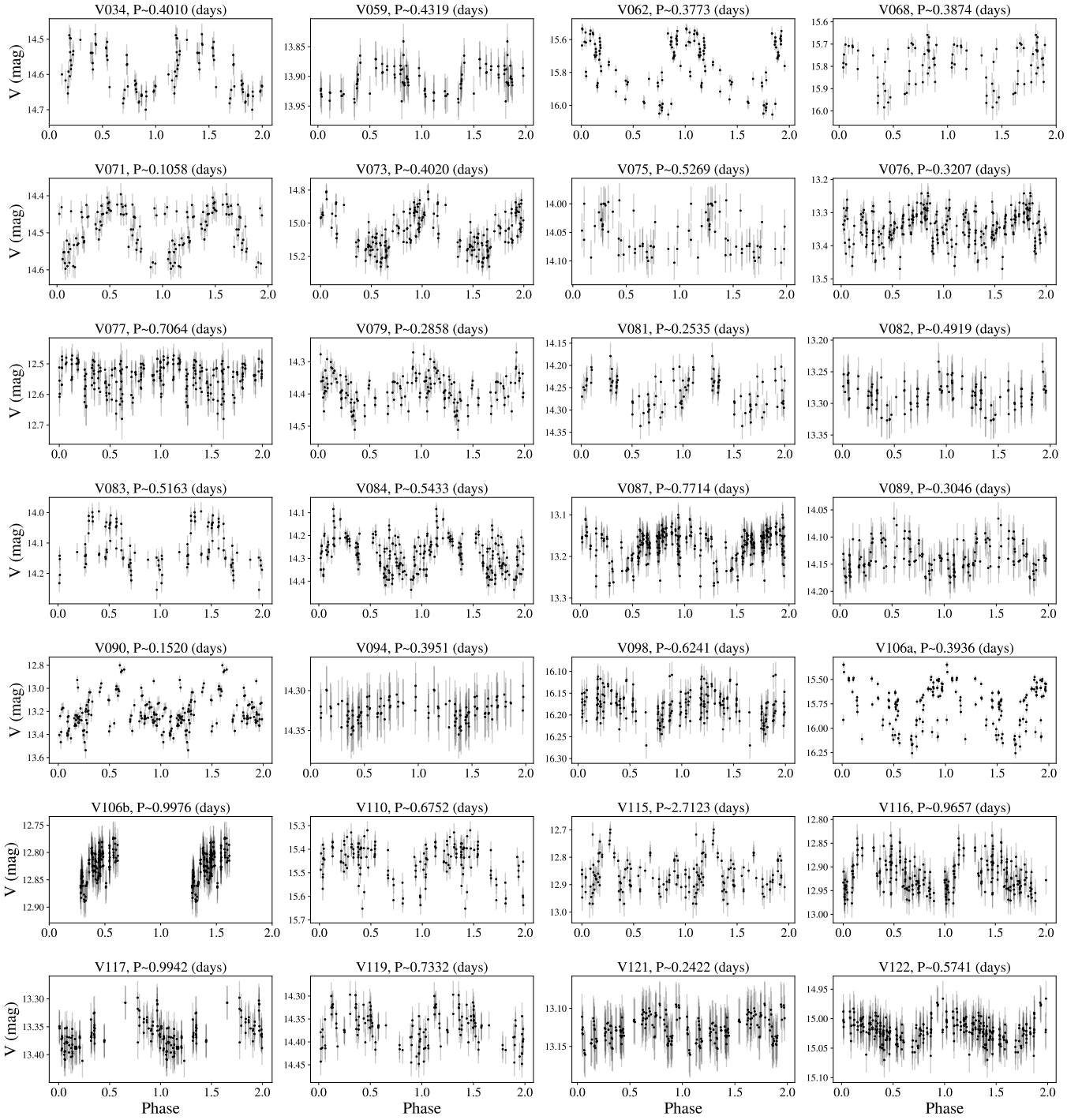

Figure 14: Stars with possible contamination ('undetermined' stars). Some of our detections had relatively large distance from known coordinates. This resulted in possible contamination by nearby stars and small SNR with relatively large intrinsic scatter. These stars are treated as a questionable, and are not processed for type classification, although some light curves indicate that they may be RRc stars by their morphology and main period. RRab stars and short-period Cepheid stars cannot be distinguished due to their common pulsation mode and inaccurate apparent magnitude. Since many of these stars don't have previously reported period values, we suggest our period estimation here.

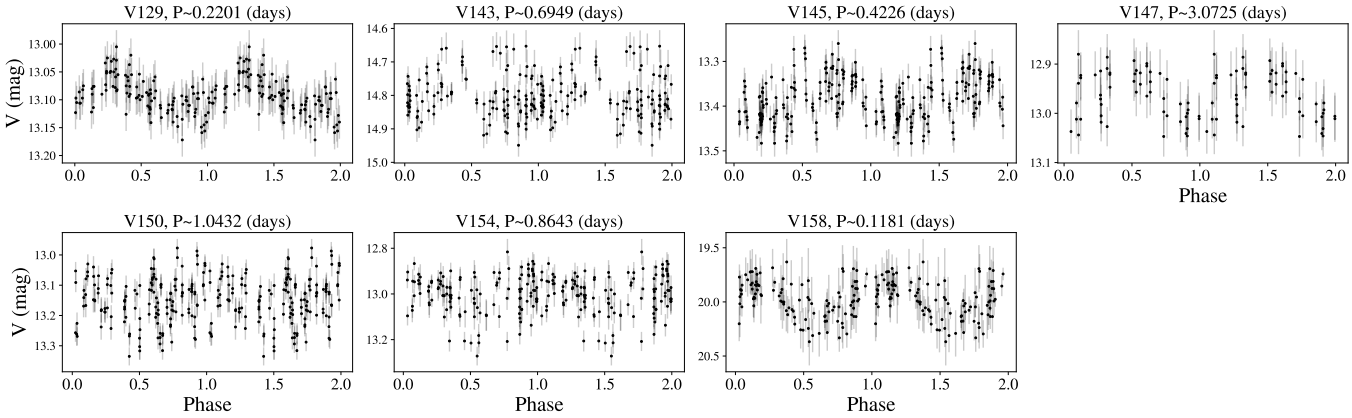

Figure 14: Stars with possible contamination ('undetermined' stars, continued)